Supplementary information

Enhancement of the thermoelectric performance via defect formation and device fabrication for $Cu_{26}Ti_2(Sb,Ge)_6S_{32}$ colusite

Koichiro Suekuni,*[,a,b] Mei Yamamoto,[a] Susumu Fujii,[c] Pierric Lemoine,[d] Philipp Sauerschnig,[e] Michihiro Ohta,[e] Emmanuel Guilmeau,[f] Michitaka Ohtaki [a,b]

[a] *Interdisciplinary Graduate School of Engineering Sciences, Kyushu University, Kasuga, Fukuoka 816-8580, Japan*

[b] *Transdisciplinary Research and Education Center for Green Technologies, Kyushu University, Kasuga, Fukuoka 816-8580, Japan*

[c] *Department of Materials, Faculty of Engineering, Kyushu University, Motooka, Fukuoka 819-0395, Japan*

[d] *Université de Lorraine, CNRS, IJL, F-54000, Nancy, France*

[e] *Global Zero Emission Research Center, National Institute of Advanced Industrial Science and Technology (AIST), Tsukuba, Ibaraki 305-8569, Japan*

[f] *CRISMAT, CNRS, Normandie Université, ENSICAEN, UNICAEN, Caen 14000, France*

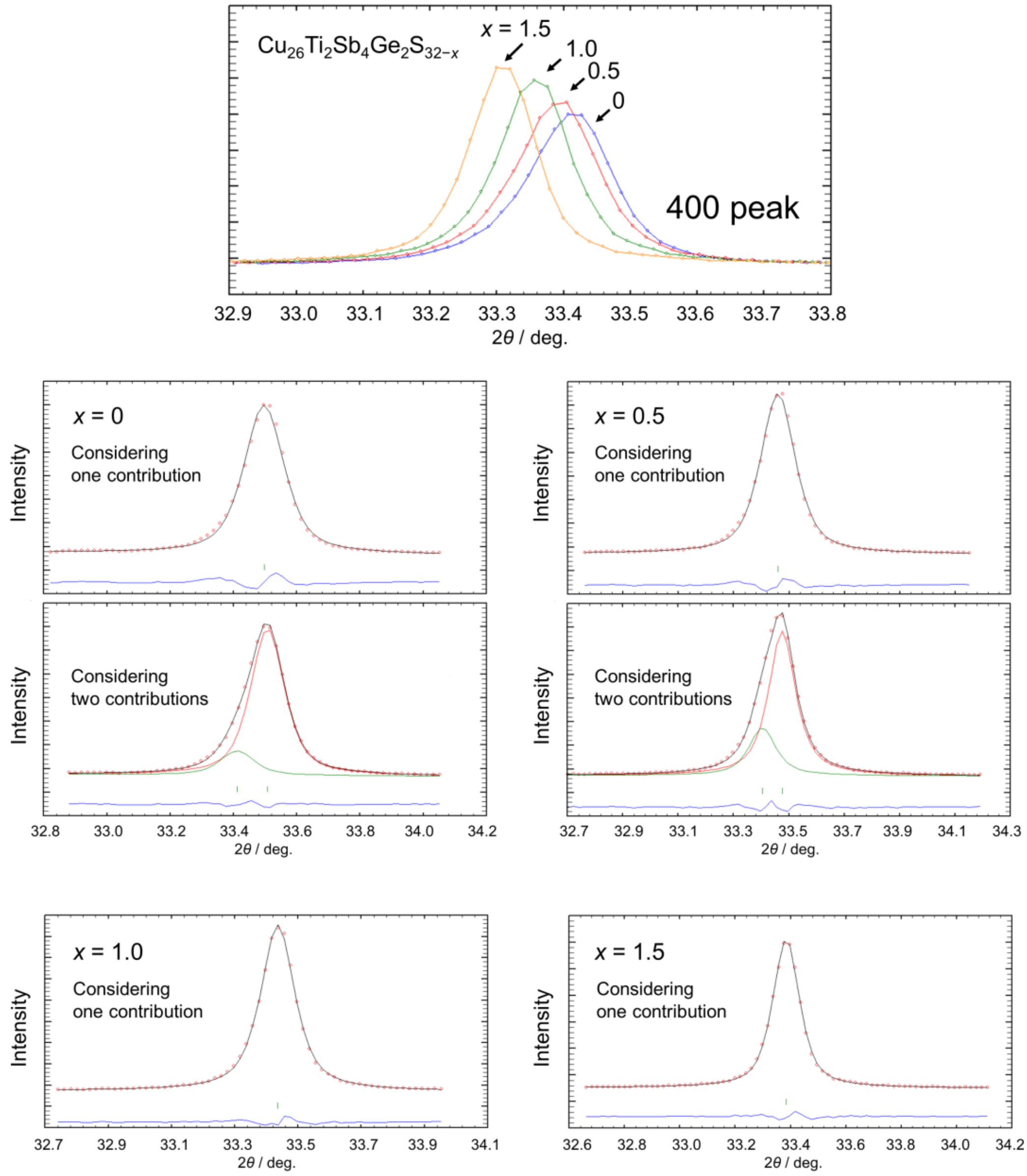

Figure S1. Powder X-ray diffraction patterns (CuKα_1) near the 400 peaks for the samples of $Cu_{26}Ti_2Sb_4Ge_2S_{32-x}$ (x = 0, 0.5, 1.0, 1.5).

Table S1. Chemical compositions for the sintered samples of $Cu_{26}Ti_2Sb_4Ge_2S_{32-x}$ (x = 0, 0.5, 1.0, 1.5). The standard deviation of the composition is given in the parentheses. Here, the total composition of Cu, Ti, Sb, and Ge was assumed to be 34. The S compositions is much smaller than the starting composition, which may be mainly due to the experimental/analytical error of the energy dispersive X-ray spectroscopy.

x	Cu	Ti	Sb	Ge	S
0	26.1(2)	1.9(1)	4.1(2)	1.8(3)	29.6(5)
0.5	26.2(2)	1.9(2)	4.2(1)	1.7(3)	29.3(3)
1.0	26.2(3)	1.8(1)	4.2(1)	1.8(3)	29.1(5)
1.5	26.1(3)	1.8(2)	4.2(1)	1.9(3)	28.5(4)

Table S2. Hole carrier concentration, n, and total thermal conductivity, κ, at room temperature for $Cu_{26}Ti_2Sb_4Ge_2S_{32-x}$.

Sample	n / 10^{21} cm^{-3}	κ / W K^{-1} m^{-1}
x = 0	3.49	2.63
x = 0.5	2.37	1.74
x = 1.0	1.77	1.42
"$Cu_{26}Ti_2Sb_4Ge_2S_{32}$" [1]	1.52	1.27
x = 1.5	0.89	0.93

[1] Hagiwara, K. Suekuni, P. Lemoine, A. R. Supka, R. Chetty, E. Guilmeau, B. Raveau, M. Fornari, M. Ohta, R. Al Rahal Al Orabi, H. Saito, K. Hashikuni and M. Ohtaki, *Chemistry of Materials*, 2021, **33**, 3449–3456.

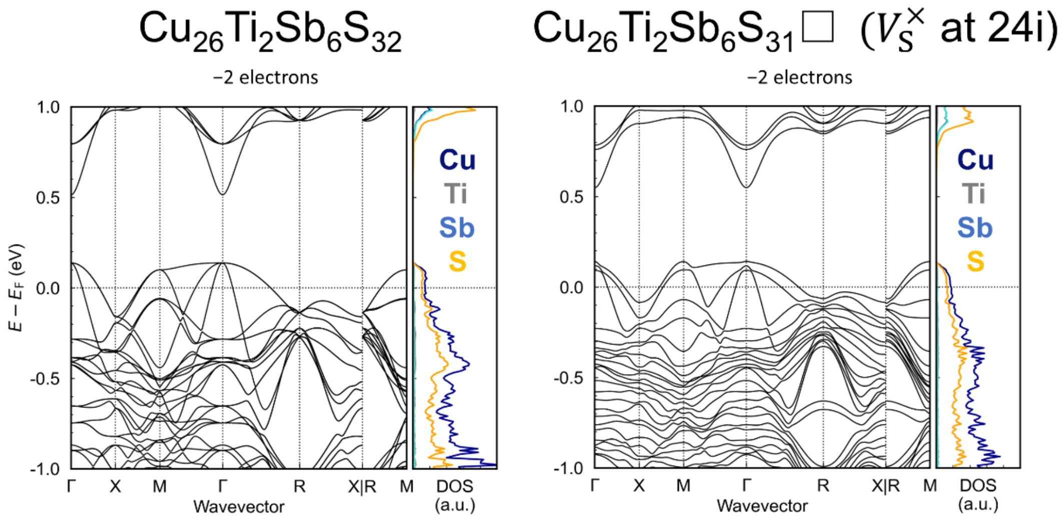

Figure S2. Electronic band dispersion relations and element-projected density of states for $Cu_{26}Ti_2Sb_6S_{32}$ and $Cu_{26}Ti_2Sb_6S_{31}$□ (see Fig. S3 for the structures).

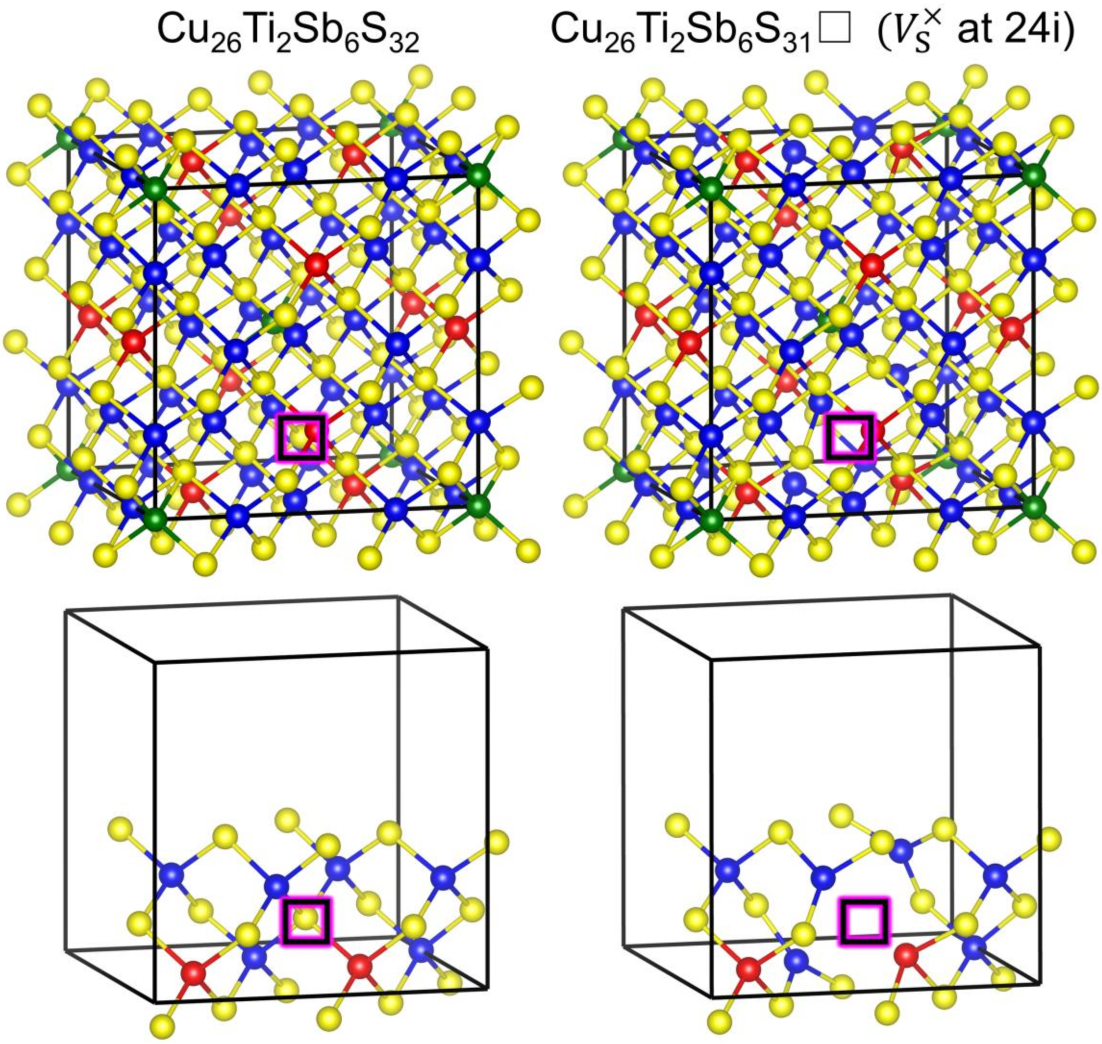

Figure S3. Relaxed structures of $Cu_{26}Ti_2Sb_6S_{32}$ and $Cu_{26}Ti_2Sb_6S_{31}\square$. For the latter, a sulphur atom was removed from the 24*i* site.

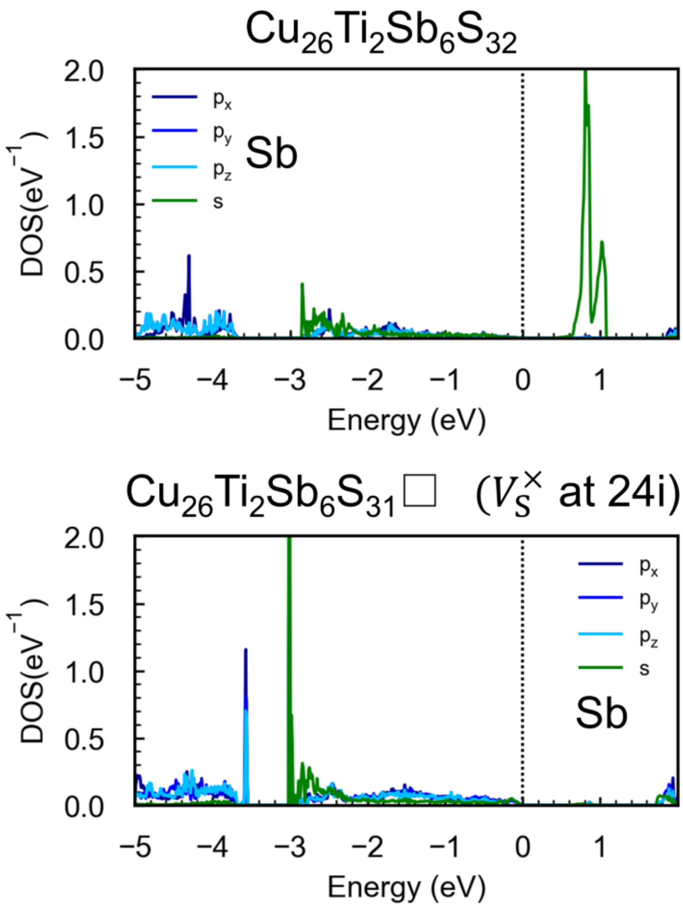

Figure S4. Orbital projected density of states of Sb for $Cu_{26}Ti_2Sb_6S_{32}$ and $Cu_{26}Ti_2Sb_6S_{31}$□. For the latter, localized states appear at −3.0 eV and −3.6 eV.

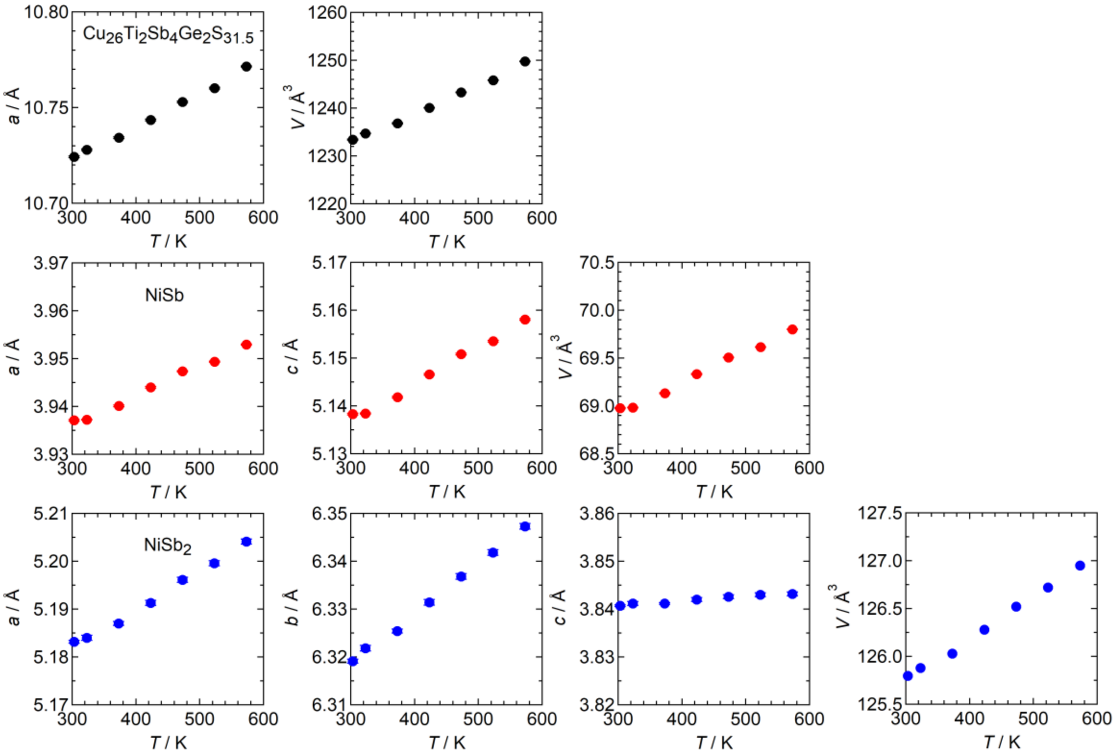

Figure S5. Temperature dependences of the lattice parameters and volume for $Cu_{26}Ti_2Sb_6S_{31.5}$ colusite, NiSb, and $NiSb_2$.

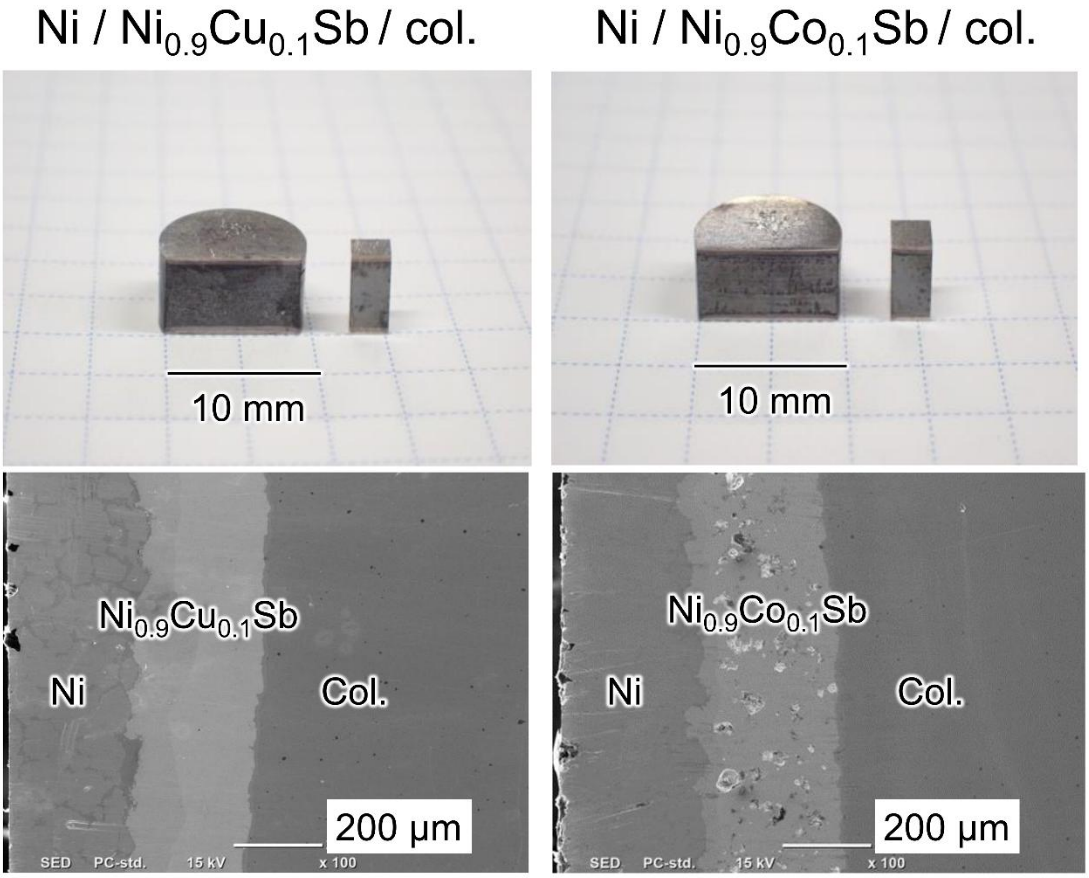

Figure S6. Sintered samples composed of (a) Ni, $Ni_{0.9}Cu_{0.1}Sb$, and $Cu_{26}Ti_2Sb_4Ge_2S_{31.5}$ (col.) layers and (b) Ni, $Ni_{0.9}Co_{0.1}Sb$, and col. layers. Secondary electron images of one end of the devices are shown at the lower panels.

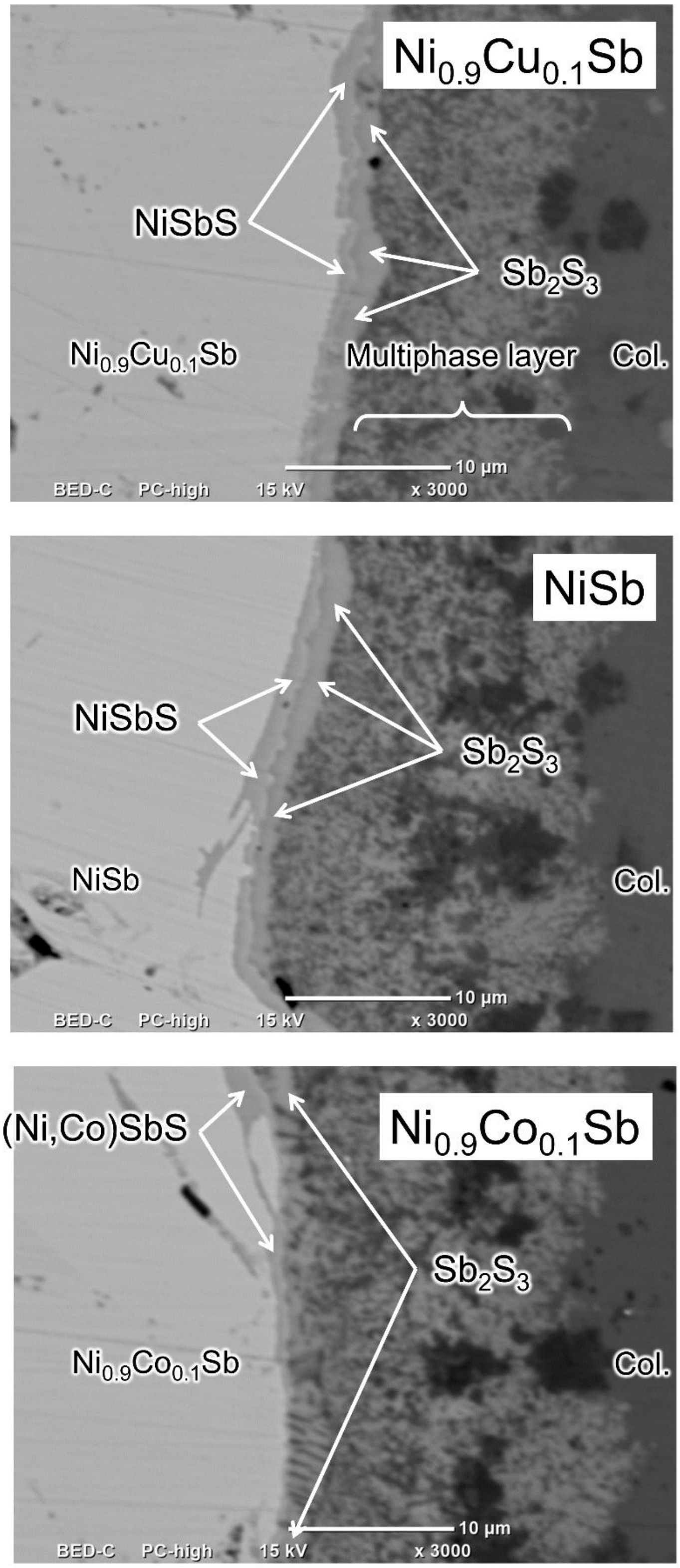

Figure S7. Secondary electron images near the interface between NiSb-based compounds and $Cu_{26}Ti_2Sb_4Ge_2S_{31.5}$ (col.) for the sintered devices.

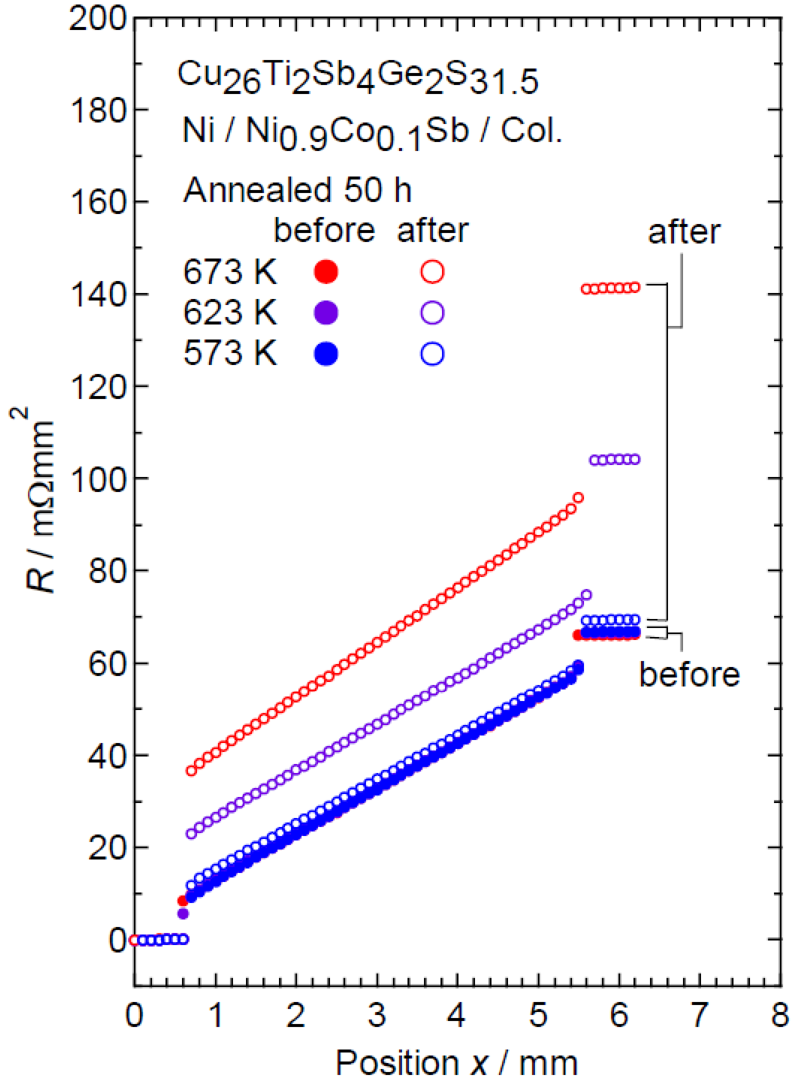

Figure S8. Cumulative electrical resistivity, *R*, for the devices composed of Ni, $Ni_{0.9}Co_{0.1}Sb$, and $Cu_{26}Ti_2Sb_4Ge_2S_{31.5}$ (col.) before and after annealing at 573 K, 623 K, and 673 K.

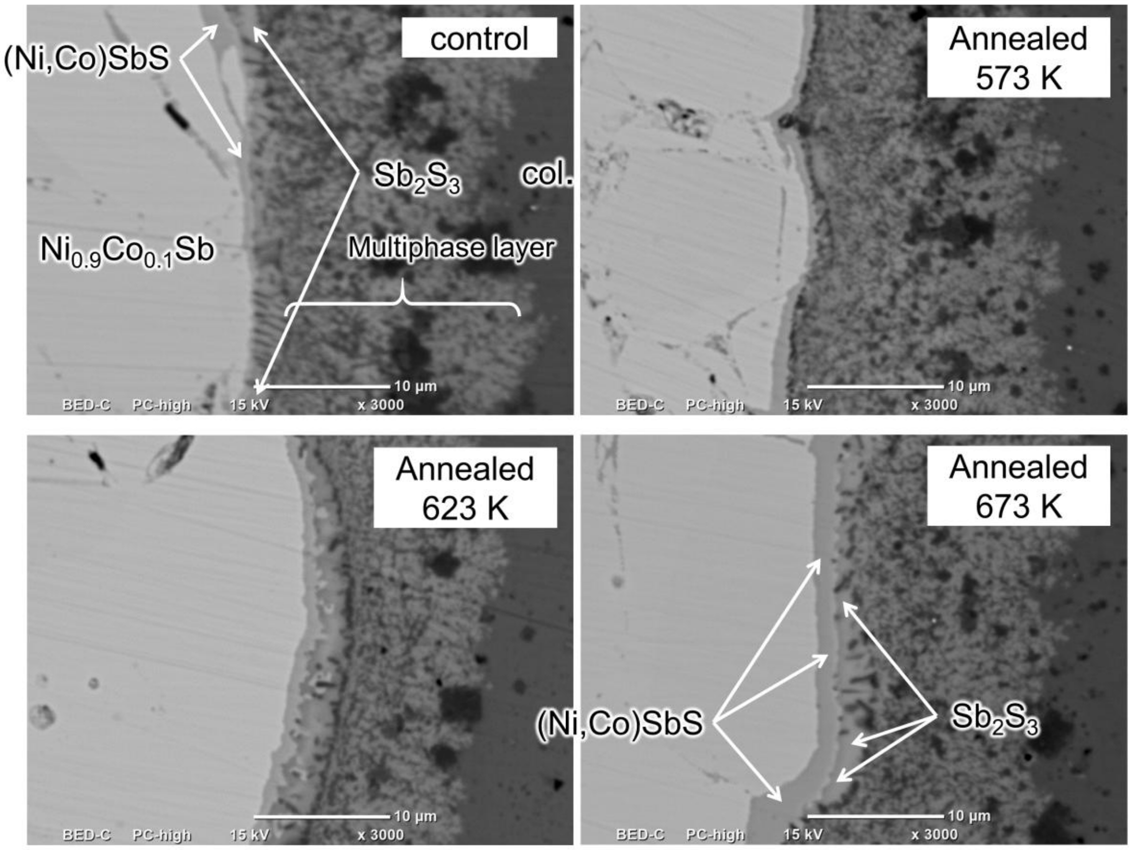

Figure S9. Secondary electron images near the interface between $Ni_{0.9}Co_{0.1}Sb$ and $Cu_{26}Ti_2Sb_4Ge_2S_{31.5}$ (col.) before and after annealing at 573 K, 623 K, and 673 K.

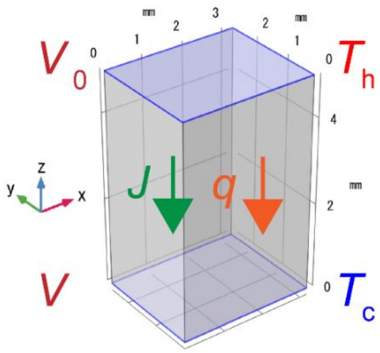

Figure S10. The model used for the finite-element method (FEM) simulation of the $Cu_{26}Ti_2Sb_4GeS_{31}$ colusite single leg thermoelectric power generation.[2] The grey surfaces are thermally and electrically insulating. Current density *J* and heat flux *q* exist perpendicular to the blue surfaces at the hot and cold ends. The voltage *V* is the electrical potential difference between the hot and cold side terminals with ground voltage V_0 ($V = 0$) on the hot side. The temperatures on the cold side T_C ~ 300 K and the hot side T_H = 368–670 K were kept constant while the current density *J* was varied to obtain the power generation characteristics.

[2] X. K. Hu, A. Yamamoto, M. Ohta, H. Nishiate; Measurement and simulation of thermoelectric efficiency for single leg, *Rev. Sci. Instrum.* **86**, 045103 (2015).

Table S3. Material′s properties (Seebeck coefficient *S*, electrical conductivity *σ*, and total thermal conductivity *κ*) and dimensions used for the finite-element method simulation of the $Cu_{26}Ti_2Sb_4GeS_{31}$ colusite single leg thermoelectric power generation.

Dimensions	mm	3.177×2.604×5.000
$S(T)$	$V\ K^{-1}$	$8.62448\times10^{-16}\ T^4 - 1.15822\times10^{-12}\ T^3 + 4.12827\times10^{-10}\ T^2 + 2.40000\times10^{-7}\ T + 1.13793\times10^{-5}$
$\sigma(T)$	$S\ m^{-1}$	$-1.44243\times10^{-6}\ T^4 + 2.88575\times10^{-3}\ T^3 - 1.95244\ T^2 + 3.35079\times10^{2}\ T + 1.14890\times10^{5}$
$\kappa(T)$	$W\ K^{-1}\ m^{-1}$	$-4.28138\times10^{-12}\ T^4 + 5.07157\times10^{-9}\ T^3 + 4.95317\times10^{-7}\ T^2 - 3.40354\times10^{-3}\ T + 2.27943$

Table S4. Finite-element method (FEM) simulation of the thermoelectric power generation of a $Cu_{26}Ti_2Sb_4GeS_{31}$ colusite single leg at hot side temperature T_H and cold side temperature T_C; open-circuit voltage V_{OC} and internal resistance R_{in}; output power *P* and heat released to the cold side Q_{out} under the condition achieving maximum conversion efficiency η_{max}.

T_H / K	T_C / K	V_{OC} / mV	R_{in} / mΩ	P / mW	Q_{out} / mW	η_{max} / %
368.8	295.3	7.69	6.12	2.40	182	1.30
466.5	296.7	19.8	6.94	14.1	404	3.38
566.5	300.2	34.2	8.07	36.4	607	5.65
670	300	51.8	9.59	71.7	817	8.08

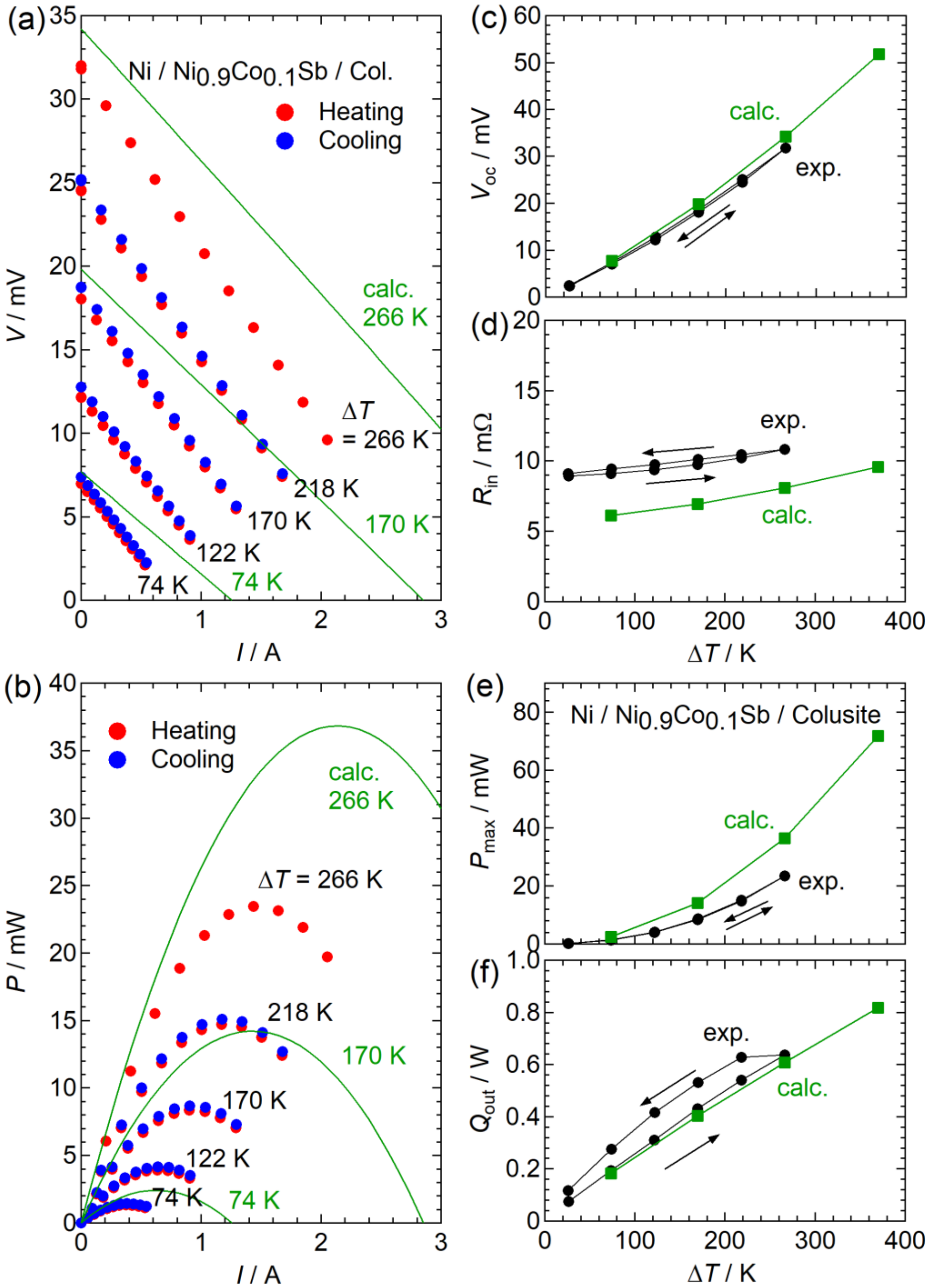

Figure S11. (a) Voltage-current (V–I) plot, (b) output power P, (c) open circuit voltage, V_{oc}, (d) internal resistance, R_{in}, and (e) output power, P_{max}, and (f) heat released into the low-temperature heat bath through the sample, Q_{out}, under the condition achieving maximum conversion efficiency η_{max} (Fig. 5e) for the device composed of Ni, $Ni_{0.9}Co_{0.1}Sb$, and $Cu_{26}Ti_2Sb_4Ge_2S_{31.5}$ (see Fig. S6). Solid lines in (a, b) and closed squares in (c–f) are the calculated data based on the thermoelectric properties of $Cu_{26}Ti_2Sb_4Ge_2S_{31}$.